Conduction-band valley spin splitting in single-layer H-Tl_2O

Yandong Ma,[1] Liangzhi Kou,[2] Aijun Du,[2] Baibiao Huang,[1] Ying Dai,[1,*] and Thomas Heine[3,†]

[1]*School of Physics, State Key Laboratory of Crystal Materials, Shandong University, Shandanan Street 27, 250100 Jinan, People's Republic of China*

[2]*School of Chemistry, Physics and Mechanical Engineering Faculty, Queensland University of Technology, Garden Point Campus, QLD 4001, Brisbane, Australia*

[3]*Wilhelm-Ostwald-Institut für Physikalische und Theoretische Chemie, Universität Leipzig, Linnéstrasse 2, 04103 Leipzig, Germany*

(Received 1 December 2017; published 31 January 2018)

Despite numerous studies, coupled spin and valley physics is currently limited to two-dimensional (2D) transition-metal dichalcogenides (TMDCs). Here, we predict an exceptional 2D valleytronic material associated with the spin-valley coupling phenomena beyond 2D TMDCs—single-layer (SL) H-Tl_2O. It displays large valley spin splitting (VSS), significantly larger than that of 2D TMDCs, and a finite band gap, which are both critically attractive for the integration of valleytronics and spintronics. More importantly, in sharp contrast to all the experimentally confirmed 2D valleytronic materials, where the strong valence-band VSS (0.15–0.46 eV) supports the spin-valley coupling, the VSS in SL H-Tl_2O is pronounced in its conduction band (0.61 eV), but negligibly small in its valence band (21 meV), thus opening a way for manipulating the coupled spin and valley physics. Moreover, SL H-Tl_2O possesses extremely high carrier mobility, as large as 9.8×10^3 cm^2 V^{-1} s^{-1}.

DOI: 10.1103/PhysRevB.97.035444

I. INTRODUCTION

Electrons in two-dimensional (2D) crystals with a hexagonal lattice are endowed with an extra valley degree of freedom in addition to charge and spin [1–3]. Such a new degree of freedom is typically robust against scattering by smooth deformations and long-wavelength phonons because the intervalley mixing requires simultaneous spin flipping and scattering from phonons [4–6]. Therefore, the valley index is particularly appealing to be used as an information carrier in next-generation electronics [7–12]. Analogous to exploiting charge for electronics or spin for spintronics, the physics of the valley will have great potential for building valleytronic devices [1–3].

For graphene, various valley-dependent electronic features have been investigated by means of theory [7–10], but the presence of inversion symmetry in its crystal structure makes both optical and electrical control of the valley index difficult. The $2H$ polytypes of 2D transition-metal dichalcogenides (TMDCs), such as monolayers and few layers of MX_2 (M = Mo, W and X = S, Se), on the other hand, provide a more applicable platform for the realization of valleytronic devices [3,13–22], taking additional advantage of the exotic spin-valley coupling phenomenon. This phenomenon can significantly suppress the spin and valley relaxations, and thus it is critically important for the observation of spin Hall effect [23], valley Hall effect [2], and optical circular dichroism [19]. Nevertheless, even though an outburst of research progress has been made on 2D TMDCs for spintronic and valleytronic applications [2,13–22], surprisingly, other 2D crystals associated with the coupled spin-valley physics are rarely reported [3].

The unusual interplay between spin and valley degrees of freedom arises from the strong valley spin splitting (VSS), in which giant spin-orbit coupling (SOC) splits the band into two subbands with spin-up and spin-down states because of the inversion symmetry breaking, and the time-reversal symmetry dictates the splitting to feature opposite signs of the two valleys where the reciprocal space vector has the opposite sign, i.e., where $\boldsymbol{K} = -\boldsymbol{K'}$ [11,15,24]. In most $2H$ 2D TMDCs, the valence band undergoes a pronounced valley spin splitting, between 0.15 eV for MoS_2 and 0.46 eV for WSe_2, whereas the conduction band is nearly spin degenerated with the size of splitting up to a few tens of meV [25,26]. With such large VSS in the valence band, the coupled spin and valley physics in 2D TMDCs has been fully characterized in experiment [17–22]. To date, the experimentally confirmed 2D valleytronic materials are all based on valence-band VSS.

Here, using first-principles calculations, we report the identification of a compelling 2D valleytronic material with spin-valley coupling in single-layer (SL) H-Tl_2O. Single-layer Tl_2O is a metal-shrouded 2D semiconductor. Its layered bulk counterpart has $1T$ symmetry [27], and its recently predicted small cleavage energy suggests that exfoliation to the monolayer is easily possible in a nonoxidative environment [28]. H-Tl_2O is a different, dynamically stable polytype, though slightly higher in energy than the $1T$ phase. It harbors a finite band gap and very large VSS, providing a highly attractive candidate material for research on valleytronics and spintronics beyond graphene and TMDCs. More intriguingly, VSS is huge in its conduction band (0.61 eV) and negligible in the valence band (21 meV), standing out in contrast to all the experimentally confirmed 2D valleytronic materials [3,23], where the strong valence-band VSS (0.15–0.46 eV) governs the coupled spin

*daiy60@sdu.edu.cn
†thomas.heine@uni-leipzig.de

and valley physics. This unique scenario for VSS not only provides a way for manipulating the spin-valley coupling, but also enriches our understanding of valley-related physics. Furthermore, H-Tl_2O possesses extremely high carrier mobility of up to 9.8×10^3 cm^2 V^{-1} s^{-1}, an order of magnitude higher than that of 2D TMDCs [29,30] and comparable to that of phosphorene [31], illustrating that it is desirable for pursuing electronic and optoelectronic applications.

II. COMPUTATIONAL METHODS

First-principles calculations are carried out using the projector-augmented-wave (PAW) method [32] as implemented in the Vienna *ab initio* simulation package (VASP) [33,34]. The Perdew-Burke-Ernzerhof (PBE) [35] functional under the generalized gradient approximation is adopted to describe the exchange and correlation interactions. Cutoff energy is set as 500 eV and the vacuum space along the z direction is set as 20 Å. Brillouin zone integration is sampled with a Monkhorst-Pack grid of $13 \times 13 \times 1$. The structure, including the lattice constant and the positions of all atoms, is relaxed until the force is less than 0.01 eV/Å. The electronic iterations convergence criterion is set as 1×10^{-6} eV. As the PBE function usually underestimates the band gap, the more reliable Heyd-Scuseria-Ernzerhof (HSE06) hybrid functional [36] is adopted for the band structure calculations. Spin-orbit coupling (SOC) is incorporated in electronic structure calculations. All results shown in this paper are based on the HSE06+SOC level, unless otherwise stated, and the results based on PBE are shown in the Supplemental Material [37]. Phonon dispersion curves are obtained using the density functional perturbation theory as implemented in the QUANTUM ESPRESSO code [38].

III. RESULTS AND DISCUSSION

Figure 1(a) shows the optimized crystal structure of SL H-Tl_2O, wherein one O atom layer is sandwiched between two layers of Tl atoms. Its structure adopts $P6$-$m2$ a symmetry with a hexagonal lattice and the inversion symmetry is broken in SL H-Tl_2O. As viewed along the x axis, the O atoms are in trigonal prismatic coordination with six Tl atoms. The structure of SL H-Tl_2O therefore can be seen as the inverse of 2D TMDCs such as H-MoS_2, where the metal atom is the central atom instead of sitting outside. The optimized lattice constants are $a = b = 3.51$ Å. SL H-Tl_2O is less stable than its T phase, but the total energies only differ by 28 meV per atom [28]. Phonon dispersion relations of SL H-Tl_2O display no imaginary frequency [see Fig. 1(b)], suggesting that it is dynamically stable.

The band structures of SL H-Tl_2O are shown in Figs. 2(a) and 2(b). Clearly, they display a semiconducting nature with an indirect band gap of 1.59 eV; i.e., it is slightly larger than that of silicon (1.1–1.4 eV) and phosphorene (1.5 eV). [39,40]. SL H-Tl_2O is an indirect semiconductor with the valence-band maximum (VBM) located at the K point; the conduction-band minimum (CBM) lies at the M point. This is unlike the case of direct band gap SL T-Tl_2O [28]. In terms of structure, SL H-Tl_2O belongs to the family of metal-shrouded 2D crystals. Recalling the fact that most of the previously reported metal-shrouded 2D crystals, such as MXenes [41]

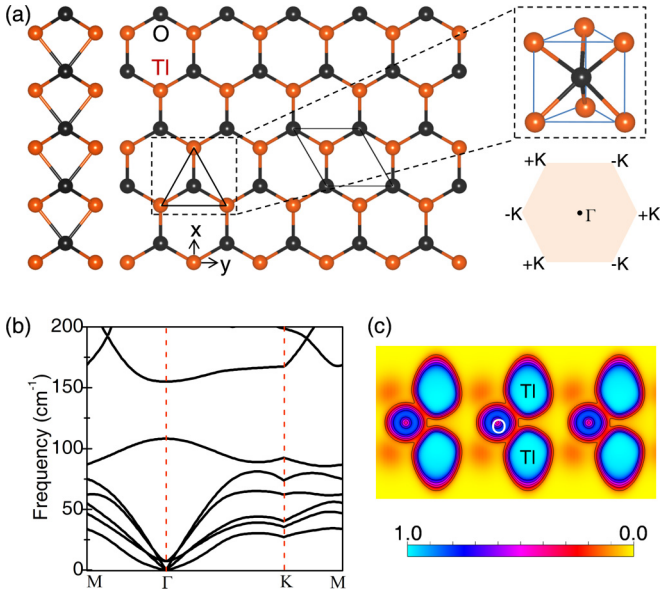

FIG. 1. (a) Side and top views of the crystal structure of SL H-Tl_2O with parallelogram marking of the unit cell. Right part in (a) shows the coordination environment of the O atom in the structure and the 2D Brillouin zone labeling the Γ point and the two inequivalent $+K$ and $-K$ points. (b) The phonon dispersion for SL H-Tl_2O. (c) Map of the electron localization function (ELF) of SL H-Tl_2O; 1 and 0 indicate the areas with strongest localization of electrons and vanishing electron density, respectively.

and alkaline earth subnitrides [42], are all metallic, both the ground state T and the H polytypes of SL TlO_2 have important distinctions as being metal-shrouded 2D semiconductors. To reflect on semiconducting physics, we analyze the bonding character in SL H-Tl_2O. The electron localization function (ELF) map in the vertical plane containing the two Tl and one O atoms is shown in Fig. 1(c). The electron localization areas are mainly distributed around Tl and O sites, while few are located around the center between them, showing an ionic character of the Tl-O bonding. Driven by the difference in electronegativity, Tl atoms give electrons to O atoms, giving rise to thallium cations and oxygen anions, respectively. While O^{2-} is the only stable oxidation state for the O element, the Tl element favors two stable oxidation states, Tl^{1+} and Tl^{3+}. The match between Tl^{1+} and O^{2-} states in SL H-Tl_2O allows the formation of the semiconducting feature.

By comparing Figs. 2(a) and 2(b), one can notice that SL H-Tl_2O exhibits the worth pursuing VSS in the presence of SOC. The detailed modification of the top valence band (TVB) and bottom conduction band (BCB) at $\pm K$ points upon VSS is plotted in Fig. 2(c). It can be clearly seen that SOC splits the spin degeneracy of TVB and BCB in the absence of inversion symmetry in SL H-Tl_2O. The time-reversal symmetry $[E_\uparrow(\mathbf{k}) = E_\downarrow(-\mathbf{k})]$ gives rise to the opposite ordering of the spin-up and spin-down states at two inequivalent valleys, K and $-K$ (the spin-orientation is out of plane). As a result, spin can be selectively excited through the optical selection rule [see Figs. 2(c) and 2(d)] [3,23]. Importantly, the splitting in BCB is exceptionally sizable, reaching 0.61 eV, which is even larger than that of the most prominent splitting in TMDCs (0.46 eV).

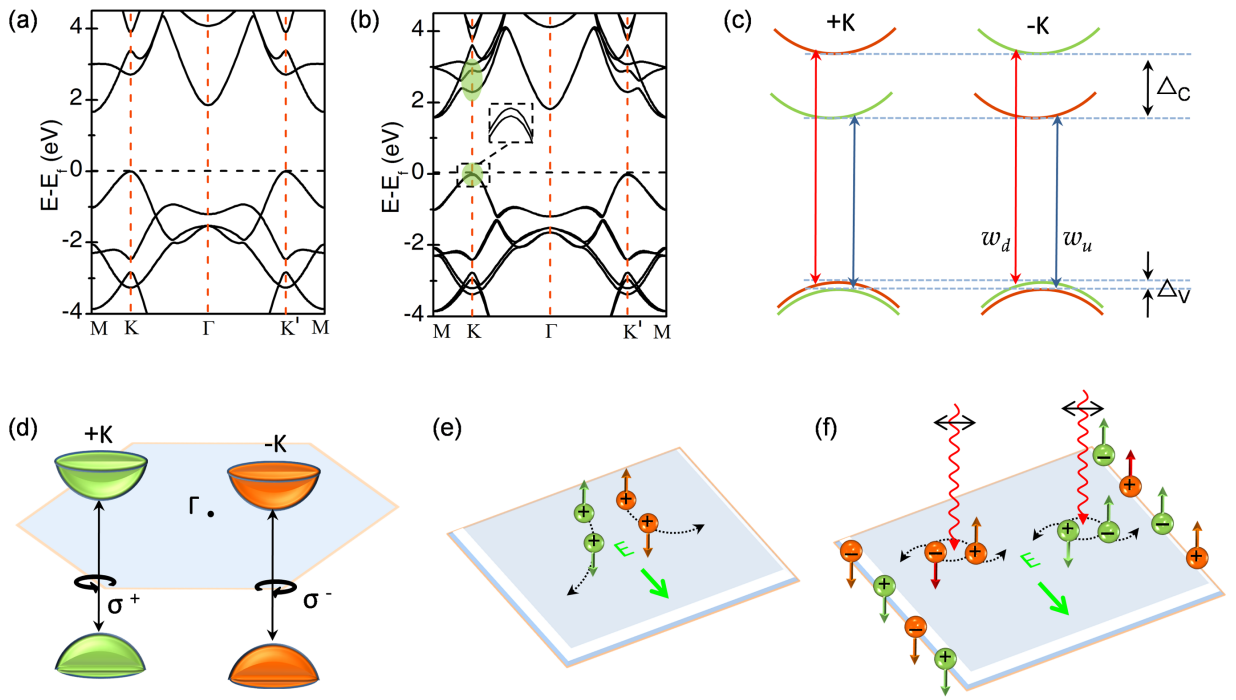

FIG. 2. Band structures of SL H-Tl_2O (a) without and (b) with SOC. Fermi level is shifted to the VBM. (c) VSS in the top valence band and the bottom conduction band at two valleys for SL H-Tl_2O. Green and red parabolas in (c) correspond to spin-up and spin-down states, respectively. (d) Simple scheme of valley-dependent optical selection rules in SL H-Tl_2O. $\sigma^{+/-}$ indicates the left- (right-) hand polarized light, which couples to the band edge transition at the $\pm K$ valley. (e) Diagram of the valley Hall effect in hole-doped SL H-Tl_2O. (f) Diagram of spin and valley Hall effects under linearly polarized optical field with frequency ω_u. Green and red balls in (e,f) correspond to the carriers in $+K$ and $-K$ valleys, respectively, and the $+$ $(-)$ symbol in the ball indicates a hole (electron).

Such a large value demonstrates its high viability for use in spintronic and valleytronic applications. In TVB, on the other hand, the spin-up and spin-down states are rather close to each other, with a separation of only 21 meV. Furthermore, the optical transition energies at the valleys [$\omega_u/\omega_d = 2.32/2.90$ eV; see Fig. 2(c)] are in the visible regime, offering experimental advantages in optical manipulation of the valley index.

To gain deeper insight into the physics of conduction-band VSS, we analyze the orbital contributions to TVB and BCB. The dominant orbital components for TVB are Tl p_z, Tl s, and O $p_{x,y}$. Provided that C_s symmetry guarantees the out-of-plane potential gradient symmetry, the VSS in SL H-Tl_2O thus mainly arises from the in-plane potential gradient asymmetries. Due to its out-of-plane orientation, the Tl p_z state has no impact on the VSS splitting, nor does the Tl s state due to its spherical symmetry ($l = 0$); hence the VSS in TVB is solely contributed by the O $p_{x,y}$ states. The weak SOC strength within the O atom leads to the obtained tiny splitting in TVB. Unlike TVB, the dominant orbital components for BCB are Tl $p_{x,y}$. The combination of the in-plane character of $p_{x,y}$ states and strong

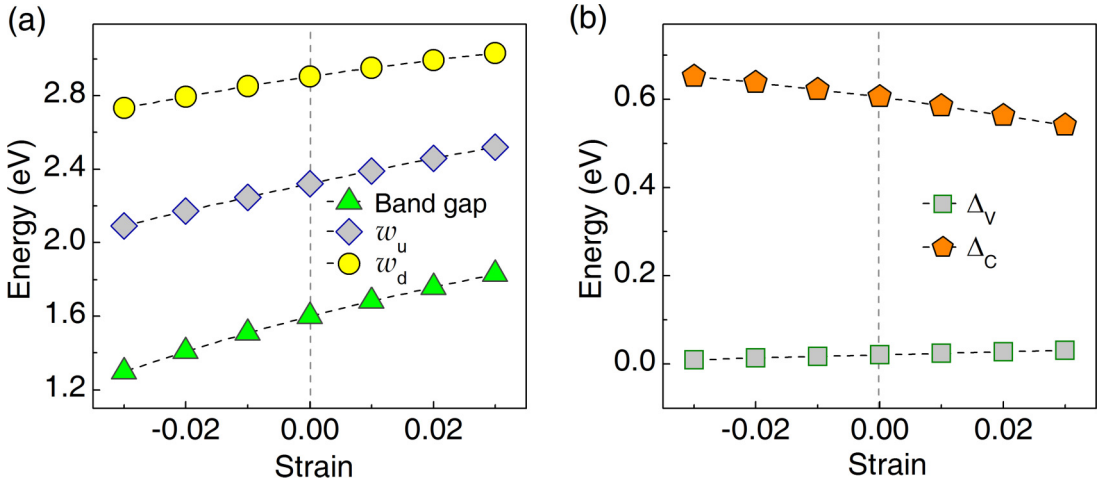

FIG. 3. (a) Strain dependence of the band gap of SL H-s_2O and the optical transition energies ω_u/ω_d [see Fig. 2(c)] for band edges. (b) Strain dependence of the VSS in TVB (Δ_V) and BCB (Δ_C).

TABLE I. Carrier mobilities and the related terms along x and y transport directions [cf. Fig. 1(a)] in SL H-Tl_2O.

	m_x^*/m_0	m_y^*/m_0	C_x (J m^{-2})	C_y (J m^{-2})	E_{lx} (eV)	E_{ly} (eV)	μ_x (cm^2 V^{-1} s^{-1})	μ_y (cm^2 V^{-1} s^{-1})
Electron	0.150	0.502	41.842	44.858	1.983	4.980	5.5×10^3	0.3×10^3
Hole	0.389	0.341	41.842	44.858	0.850	0.889	8.7×10^3	9.7×10^3

SOC strength within the Tl atom results in the substantial VSS in the conduction band. The inverse behavior, large VSS in the valence band, in 2D TMDCs is ascribed to the fact that the Mo d_{3z2-r2} states with out-of-plane character and the Mo d_{x2-y2}/d_{xy} states with in-plane character govern BCB and TVB, respectively [15].

Figure 3 shows the effect of strain on the unique properties of SL H-Tl_2O. As shown in Fig. 3(a), the band gap and optical transition energies (ω_u/ω_d) increase monotonically with strain. Specifically, ω_u/ω_d changes from 2.09/2.73 eV at -3% to 2.52/3.03 eV at 3%, but, importantly, still remains in the visible light range. The band gap increases from 1.30 eV at -3% to 1.83 eV at 3% and indirect and close to the optimal value for a photovoltaic absorber. Compared with the band gap and optical transition energies, the magnitudes of the VSS in both TVB (Δ_V) and BCB (Δ_C) are relatively insensitive to strain [see Fig. 3(b)]. For example, Δ_V increases from 10 meV at -3% to 31 meV at 3%, while Δ_C decreases slightly from 0.65 eV at -3% to 0.54 meV at 3%. The above results clearly indicate that the significant VSS in the conduction band as well as optical transition energies for SL H-Tl_2O are robust against mechanical deformation, which is desirable for realistic applications.

It has been well established that the carriers at inequivalent valleys are subjected to opposite Berry curvatures. By applying an in-plane electric field, the carrier will obtain a velocity proportional to the Berry curvature, yielding a Hall current with a sign relying on the valley; this is the valley Hall effect [3,23]. Obviously, at equilibrium, SL H-Tl_2O could not exhibit the valley Hall effect, and carrier doping to the valleys is necessary. Similar to the case of SL WSe_2 [15], hole doping to the valleys could be easily achieved in SL H-Tl_2O, whereas electron doping to valleys is nearly unattainable as the bands at the Γ point will interfere with it; see Fig. 2(b). The valley Hall effect in hole-doped SL H-Tl_2O is described in Fig. 2(e), in which the doped holes from different valleys move to opposite boundaries of the sample upon applying an in-plane electric field.

Compared with hole doping, optical illumination can lead to more interesting phenomena. Employing optical illumination with different circular polarizations and frequencies, we can selectively excite carriers with different combinations of spin and valley indexes [10,11]. For example, as shown in Fig. 2(d), under the excitation with left-hand polarized light with frequency ω_u, spin-up electrons and spin-down holes can be generated in valley $+K$. While under the excitation with right-hand polarized light with frequency ω_u, spin-down electrons and spin-up holes can be generated in valley $-K$. This optical selection rule can generate long-lived spin and valley. Furthermore, under the excitation with linearly polarized optical field with frequency ω_u, the spin-up (spin-down) electrons and spin-down (spin-up) holes will be generated in valley $+K$ ($-K$) of SL H-Tl_2O, which originates from the valley optical selection rule. Due to the opposite Berry curvatures in TVB and BCB, the excited electrons and holes in the same valley will also acquire opposite transverse velocities under an in-plane electric field. As illustrated in Fig. 2(f), the spin-up electrons (holes) from valley $+K$ ($-K$) are accumulated at one boundary, and the spin-down holes (electrons) from valley $+K$ ($-K$) are accumulated at the opposite boundary. This results in both the spin and valley Hall currents, allowing the coexistence of spin and valley Hall effects in SL H-Tl_2O. It is worth emphasizing that, at a given boundary, recommendation between electron and hole is forbidden, because both flip spin and valley indices are required. This strong valley-spin coupling in SL H-Tl_2O can further protect each index.

Finally we discuss the transport properties of SL H-Tl_2O. It can be seen clearly from Fig. 2(c) that the band edges of SL H-Tl_2O exhibit a strong dispersion owing to the dispersive s and p states, strongly suggesting that the carriers would be very light. Table I summarizes the calculated carrier effective masses of SL H-Tl_2O. As expected, the electron (hole) effective masses along the x/y direction are only $0.150/0.502\,m_0$ ($0.389/0.341\,m_0$), where m_0 is the mass of a free electron. We then calculate its carrier mobility as listed in Table I. The electrons in SL H-Tl_2O display an interesting anisotropic transport behavior with an electron along the x direction (5.5×10^3 cm^2 V^{-1} s^{-1}) being more mobile than that along the y direction (0.3×10^3 cm^2 V^{-1} s^{-1}). On the other hand, holes are highly mobile along both the x and y directions ($8.7 \times 10^3/9.7 \times 10^3$ cm^2 V^{-1} s^{-1}), which is even comparable to the mobility of phosphorene [30]. As a consequence, there would be a good separation between electrons and holes in terms of their large mobility difference along the y direction, whereas no such separation can be observed along the x direction.

IV. CONCLUSION

In conclusion, we demonstrate that SL H-Tl_2O is a promising 2D valleytronic material beyond 2D TMDCs, owning to its large VSS and finite band gap which are critically attractive for valleytronic and spintronic applications. The VSS in SL H-Tl_2O is significantly larger than that of widely studied 2D TMDCs. Interestingly, such a pronounced VSS in SL H-Tl_2O is not common for the conduction band in a single-layer 2D valleytronic material. Additionally, SL H-Tl_2O possesses distinct carrier mobilities that are higher than 2D TMDCs and even comparable to those of phosphorene. Our results not only highlight an interesting 2D valleytronic material but also open an alternative way for manipulating the coupled spin and valley physics. Though this is a hypothetical material suggestion, the rapid development of experimental techniques for fabrication of low-dimensional materials makes us believe that the SL H-Tl_2O can soon be obtained experimentally.

ACKNOWLEDGMENTS

Financial support by the Deutsche Forschungsgemeinschaft (DFG, HE 3543/27-1), National Basic Research Program of China (Grant No. 2013CB632401), National Natural Science Foundation of China (Grant No. 11374190), Program of Introducing Talents of Discipline to Universities (111 Program, Grant No. 297B13029), and the high-performance computing resources of ZIH Dresden are gratefully acknowledged. We thank Professor Udo Schwingenschlögl for fruitful discussions. We also thank the Taishan Scholar Program of Shandong Province and Qilu Young Scholar Program of Shandong University.

The authors declare no competing financial interests.

[1] A. H. Castro Neto, F. Guinea, N. M. R. Peres, K. S. Novoselov, and A. K. Geim, Rev. Mod. Phys. **81**, 109 (2009).
[2] K. F. Mak, K. L. McGill, J. Park, and P. L. McEuen, Science **344**, 1489 (2014).
[3] J. R. Schaibley, H. Y. Yu, G. Clark, P. Rivera, J. S. Ross, K. L. Seyler, W. Yao, and X. D. Xu, Nat. Rev. Mater. **1**, 16055 (2016).
[4] T. C. Berkelbach, M. S. Hybertsen, and D. R. Reichman, Phys. Rev. B **88**, 045318 (2013).
[5] H.-Z. Lu, W. Yao, D. Xiao, and S.-Q. Shen, Phys. Rev. Lett. **110**, 016806 (2013).
[6] O. L. Sanchez, D. Ovchinnikov, S. Misra, A. Allain, and A. Kis, Nano Lett. **16**, 5792 (2016).
[7] A. Rycerz, J. Tworzydlo, and C. W. J. Beenakker, Nat. Phys. **3**, 172 (2007).
[8] A. R. Akhmerov and C. W. J. Beenakker, Phys. Rev. Lett. **98**, 157003 (2007).
[9] D. Xiao, W. Yao, and Q. Niu, Phys. Rev. Lett. **99**, 236809 (2007).
[10] W. Yao, D. Xiao, and Q. Niu, Phys. Rev. B **77**, 235406 (2008).
[11] D. Xiao, G.-B. Liu, W. Feng, X. Xu, and W. Yao, Phys. Rev. Lett. **108**, 196802 (2012).
[12] Y. J. Zhang, T. Oka, R. Suzuki, J. T. Ye, and Y. Iwasa, Science **344**, 725 (2014).
[13] X. F. Chen, L. H. Zhong, X. Li, and J. S. Qi, Nanoscale **9**, 2188 (2017).
[14] Y. C. Cheng, Q. Y. Zhang, and U. Schwingenschlögl, Phys. Rev. B **89**, 155429 (2014).
[15] Z. Y. Zhu, Y. C. Cheng, and U. Schwingenschlögl, Phys. Rev. B **84**, 153402 (2011).
[16] N. Singh and U. Schwingenschlögl, Adv. Mater. **29**, 1600970 (2017).
[17] K. F. Mak, K. He, J. Shan, and T. F. Heinz, Nat. Nanotechnol. **7**, 494 (2012).
[18] H. Zeng, J. Dai, W. Yao, D. Xiao, and X. Cui, Nat. Nanotechnol. **7**, 490 (2012).
[19] T. Cao, G. Wang, W. P. Han, H. Q. Ye, C. R. Zhu, J. R. Shi, Q. Niu, P. H. Tan, E. G. Wang, B. L. Liu, and J. Feng, Nat. Commun. **3**, 887 (2012).
[20] A. M. Jones, H. Y. Yu, N. J. Ghimire, S. F. Wu, G. Aivazian, J. S. Ross, B. Zhao, J. Q. Yan, D. G. Mandrus, D. Xiao, W. Yao, and X. D. Xu, Nat. Nanotechnol. **8**, 634 (2013).
[21] B. R. Zhu, H. L. Zeng, J. F. Dai, Z. R. Gong, and X. D. Cui, Proc. Natl. Acad. Sci. USA **111**, 11606 (2014).
[22] Y. W. Zhang, H. Li, M. Wang, R. Liu, S. L. Zhang, and Z. J. Qiu, ACS Nano **9**, 8514 (2015).
[23] J. Wunderlich, B. Kaestner, J. Sinova, and T. Jungwirth, Phys. Rev. Lett. **94**, 047204 (2005).
[24] X. D. Xu, W. Yao, D. Xiao, and T. F. Heinz, Nat. Phys. **10**, 343 (2014).
[25] A. Kormanyos, V. Zolyomi, N. D. Drummond, P. Rakyta, G. Burkard, and V. I. Falko, Phys. Rev. B **88**, 045416 (2013).
[26] H. Ochoa, F. Finocchiaro, F. Guinea, and V. I. Falko, Phys. Rev. B **90**, 235429 (2014).
[27] H. Sabrowsky, Z Anorg. Allg. Chem. **381**, 266 (1971).
[28] Y. D. Ma, A. Kuc, and T. Heine, J. Am. Chem. Soc. **139**, 11694 (2017).
[29] B. Radisavljevic, A. Radenovic, J. Brivio, V. Giacometti, and A. Kis, Nat. Nanotechnol. **6**, 147 (2011).
[30] H.-J. Chuang, X. Tan, N. J. Ghimire, M. M. Perera, B. Chamlagain, M. M. Cheng, J. Yan, D. Mandrus, D. Tomanek, and Z. Zhou, Nano Lett. **14**, 3594 (2014).
[31] J. Qiao, X. Kong, Z.-X. Hu, F. Yang, and W. Ji, Nat. Commun. **5**, 4475 (2014).
[32] P. E. Blöchl, Phys. Rev. B **50**, 17953 (1994).
[33] G. Kresse and J. Furthmüller, Comput. Mater. Sci. **6**, 15 (1996).
[34] G. Kresse and J. Furthmüller, Phys. Rev. B **54**, 11169 (1996).
[35] J. P. Perdew, K. Burke, and M. Ernzerhof, Phys. Rev. Lett. **77**, 3865 (1996).
[36] J. Heyd, G. E. Scuseria, and M. Ernzerhof, J. Chem. Phys. **118**, 8207 (2013).
[37] See Supplemental Material at http://link.aps.org/supplemental/10.1103/PhysRevB.97.035444 for computational methods, band structures under different strain, band structures using PBE, and the transport properties calculated using PBE. This material is available free of charge via the Internet.
[38] P. Giannozzi, S. Baroni, N. Bonini, M. Calandra, R. Car, C. Cavazzoni, D. Ceresoli, G. L. Chiarotti, M. Cococcioni, I. Dabo *et al.*, J. Phys.: Condens. Matter **21**, 395502 (2009).
[39] Q. H. Wang, K. Kalantar-Zadeh, A. Kis, J. N. Coleman, and M. S. Strano, Nat. Nanotechnol. **7**, 699 (2012).
[40] H. Liu, A. T. Neal, Z. Zhu, Z. Luo, X. Xu, D. Tomanek, and P. D. Ye, ACS Nano **8**, 4033 (2014).
[41] B. Anasori, M. R. Lukatskaya, and Y. Gogotsi, Nat. Rev. Mater. **2**, 16098 (2017).
[42] K. Lee, S. W. Kim, Y. Toda, S. Matsuishi, and H. Hosono, Nature **494**, 336 (2013).